GNSS characterization of hydrological loading in South and Southeast Asia

Materna, Kathryn; Feng, Lujia; Lindsey, Eric O.; Hill, Emma M.; Ahsan, Aktarul; Khorshed Alam, A. K. M.; Kyaw, Moe Oo; Than, Oo; Aung, Thura; Ngwe Khaing, Saw; Bürgmann, Roland

2020

Materna, K., Feng, L., Lindsey, E. O., Hill, E. M., Ahsan, A., Khorshed Alam, A. K. M., Kyaw, M. O., Than, O., Aung, T., Ngwe Khaing, S. & Bürgmann, R. (2020). GNSS characterization of hydrological loading in South and Southeast Asia. Geophysical Journal International, 224(3), 1742-1752. https://dx.doi.org/10.1093/gji/ggaa500

https://hdl.handle.net/10356/148918

https://doi.org/10.1093/gji/ggaa500

Supplementary Material for:
GNSS characterization of hydrological loading in South and Southeast Asia

Kathryn Materna[1*], Lujia Feng[2], Eric O. Lindsey[2], Emma M. Hill[2,3], Aktarul Ahsan[4], A. K. M. Khorshed Alam[5], Kyaw Moe Oo[6], Oo Than[6], Thura Aung[7], Saw Ngwe Khaing[8], Roland Bürgmann[1,9]

1. Berkeley Seismology Laboratory, Berkeley, California, USA
2. Earth Observatory of Singapore, Nanyang Technological University, Singapore
3. Asian School of the Environment, Nanyang Technological University, Singapore
4. Geological Survey of Bangladesh, Bangladesh
5. Formerly at Geological Survey of Bangladesh, Bangladesh
6. Department of Meteorology and Hydrology, Myanmar
7. Myanmar Earthquake Committee
8. Department of Geology, Hinthada University, Hinthada, Myanmar
9. UC Berkeley Earth and Planetary Science Department, Berkeley, California, USA

*now at Earthquake Science Center, US Geological Survey, Moffett Field, California, USA

Contents:

Text S1

For performing the synthetic calculation shown in Figure 6, we distributed ~14000 disk loads according to the locations of rivers and lakes in SE Asia that were identified using a 1-arc-minute water mask; we then applied spatial loads of 6 km radius (matching our PREM Green's function for the rest of the computation) and height of 17 cm of water on each of those disks. The total imposed volume is 300 km^3, roughly equivalent to the excess discharge in the Ganges river during the monsoon season (Jian et al., 2009). This is intended as an order-of-magnitude calculation rather than an exact budget of the hydrological cycle.

Jian, J., Webster, P. J., & Hoyos, C. D. (2009). Large-scale controls on the Ganges and Brahaputra river discharge on intraseasonal and seasonal time-scales. *Quarterly Journal of the Royal Meterological Society*, *135*, 353–370.

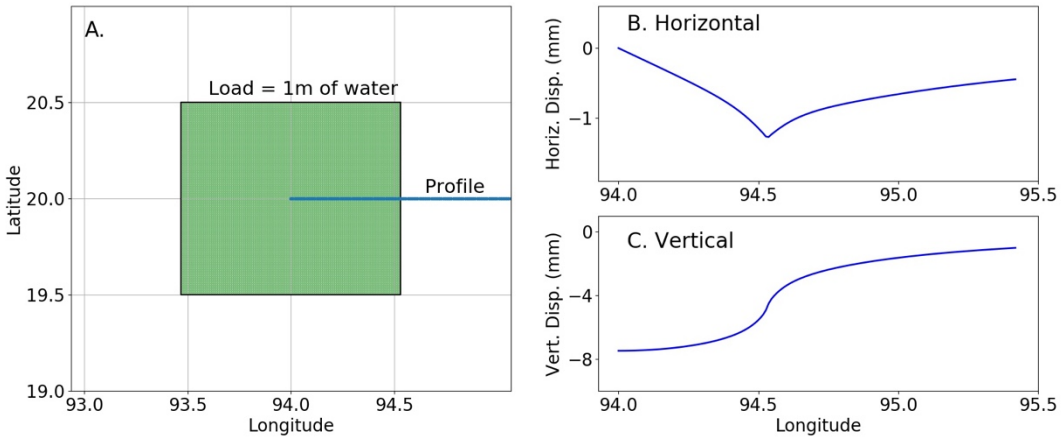

Figure S1: An example of a 1° x 1° loading calculation on a PREM earth structure. The maximum vertical deformation due to the load is several times larger than the maximum horizontal deformation.

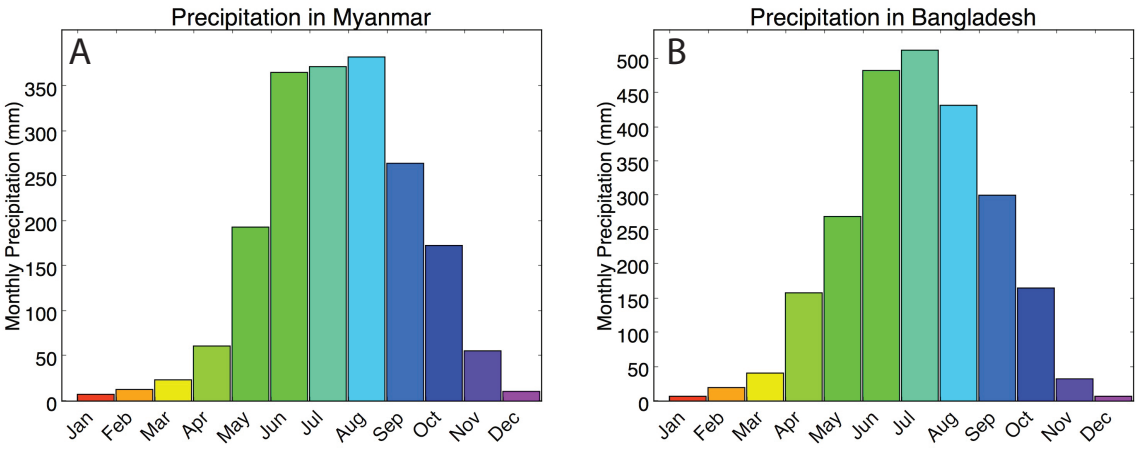

Figure S2: Average monthly precipitation in Myanmar and Bangladesh (World Bank Group Climate Change Knowledge Portal, 2010).

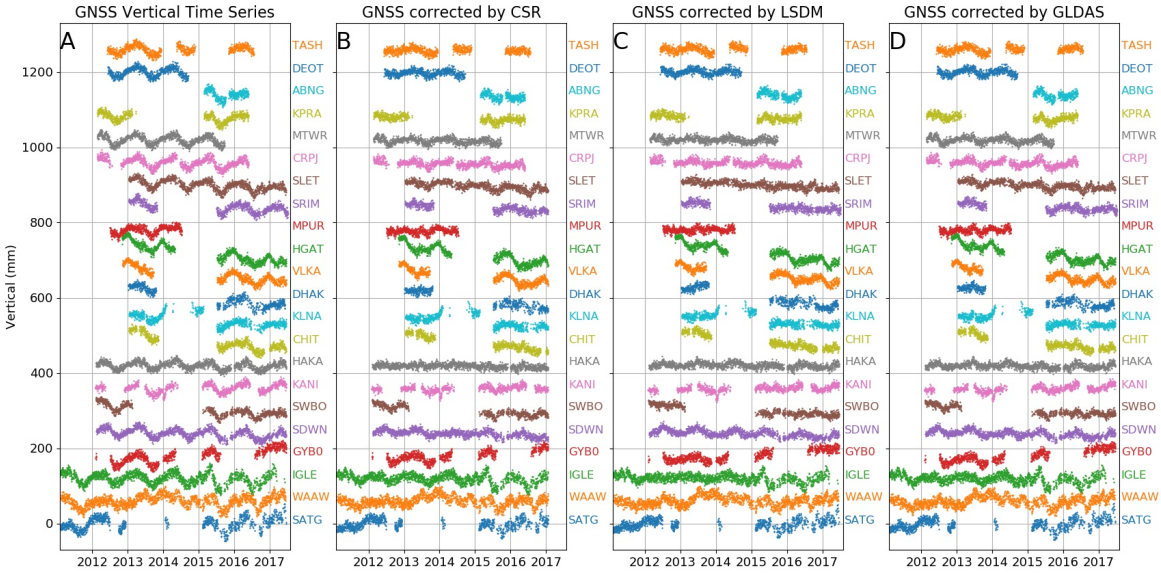

Figure S3: Vertical GNSS time series at the MIBB network, corrected for hydrological loading using each of the models explored in this paper.

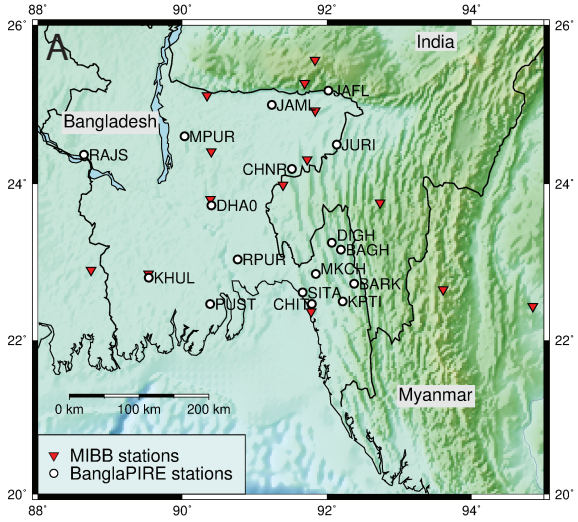

Figure S4: Map of the BanglaPIRE GNSS network.

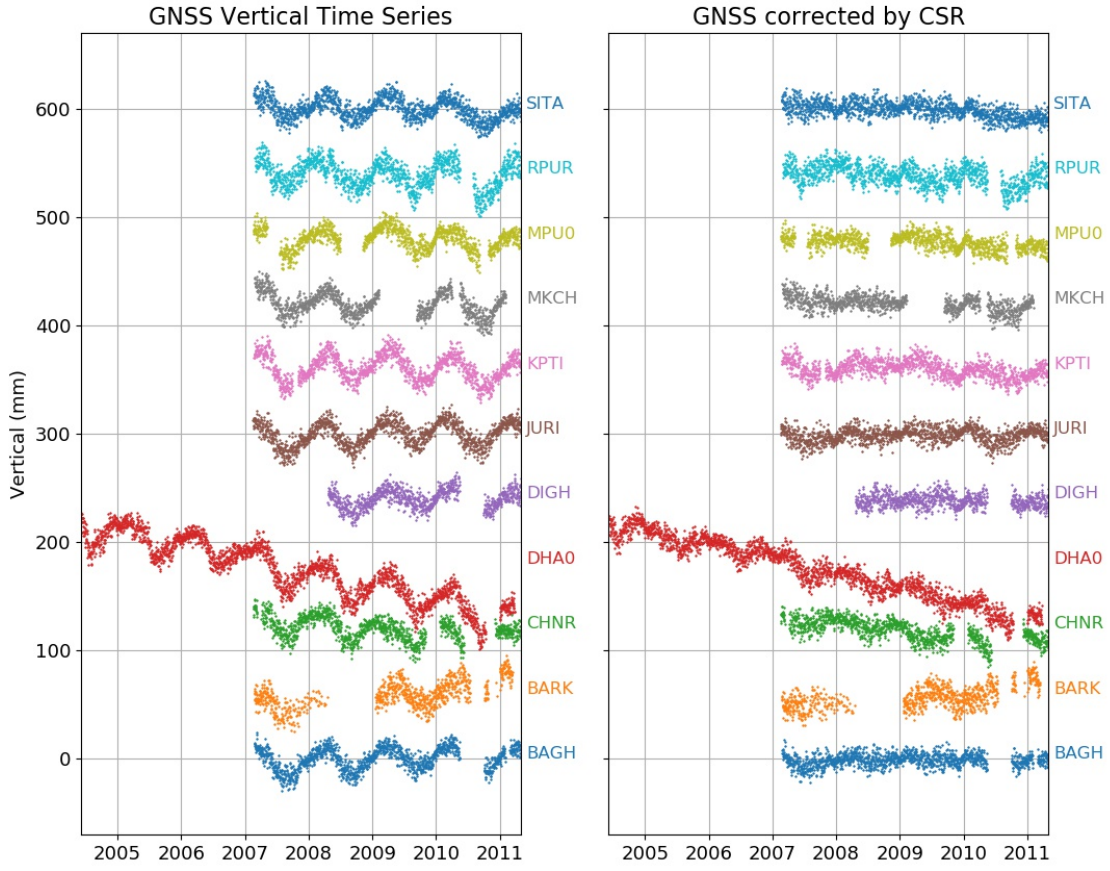

Figure S5: Vertical data at the BanglaPIRE GNSS stations showing the corrected GNSS time series after applying a GRACE-based hydrological loading model.

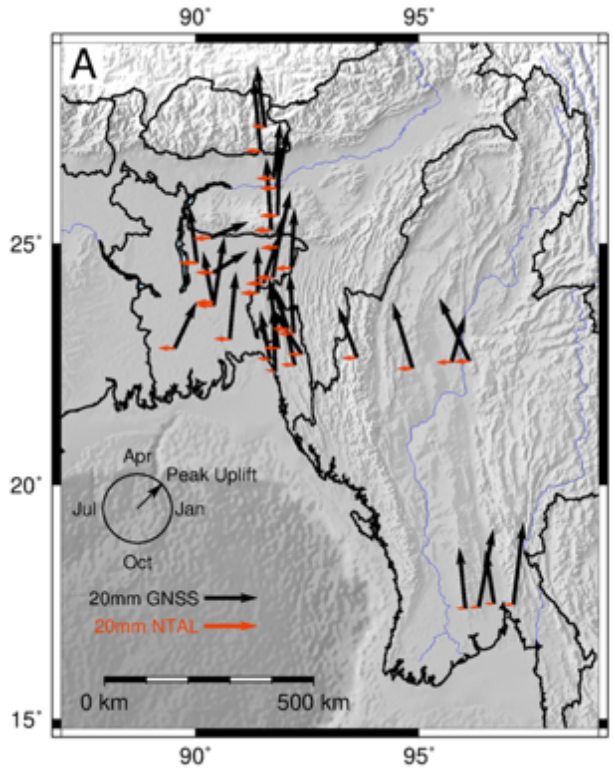

Figure S6: Phasor diagram for the raw GNSS time series before correction of non-tidal atmospheric and non-tidal ocean loading. The orange vectors are the phasors for the applied non-tidal ocean and atmosphere correction. The ocean and atmosphere loading is small and has peak uplift around July, which is consistent with a low-pressure system at the time of the monsoon.

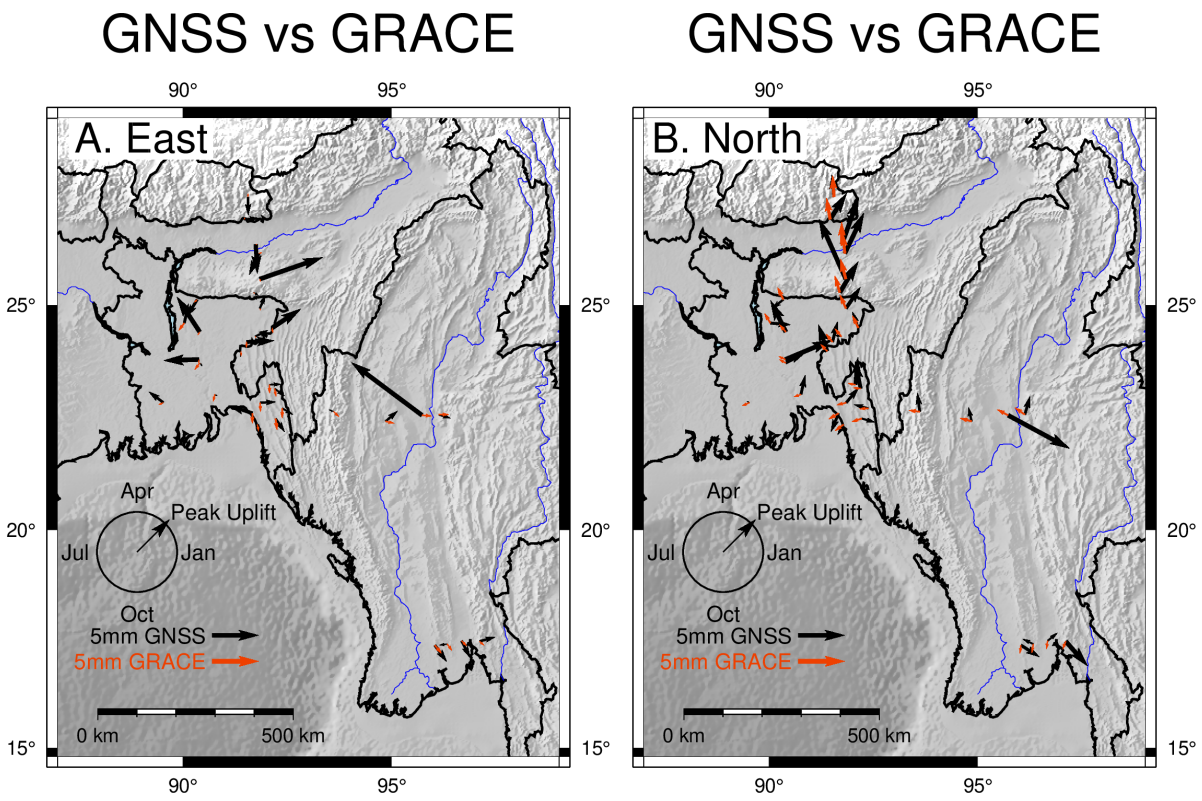

Figure S7: Estimated phase and amplitude of horizontal seasonal oscillations in the GNSS data (black) and the GRACE models (orange).

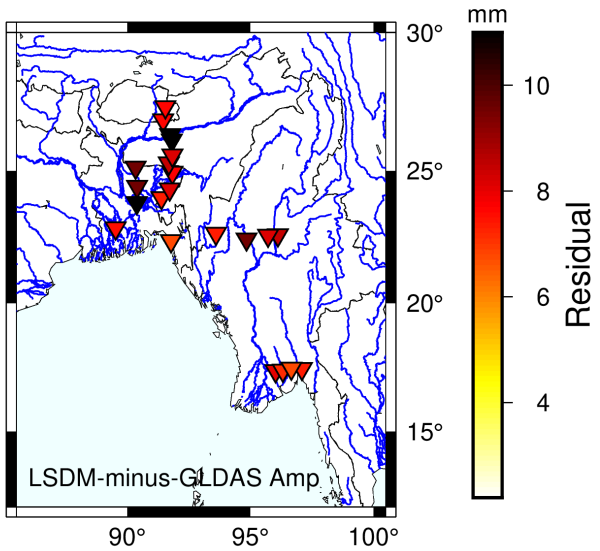

Figure S8: The amplitude difference between LSDM and GLDAS model predictions at each station in the MIBB network. The differences between these models is hypothesized to be the loading component from rivers and lakes. The scale bar is the same as Figure 6a.

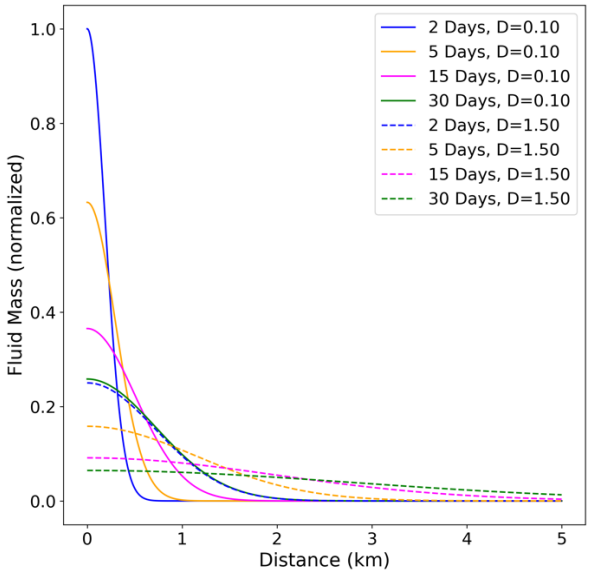

Figure S9: Diffusion curves for a sudden influx of surface water diffusing into the subsurface. D is the hydraulic diffusivity. The normalized flux on the y axis is unitless. Hydraulic diffusivities of this range are consistent with sandstone, basalt, chalk, and karst and inconsistent with granite, marble, and clay (Barbour and Wyatt, 2014). In a time period of 15-30 days, water could reach a subsurface aquifer at several kilometers' depth but could not move significant distances laterally.

Station (Network)	**Reason**
DRNG (MIBB)	Time series is mostly gaps
ICHA (MIBB)	Insufficient data length
BNGM (BanglaPIRE)	Insufficient data length
CHI0 (BanglaPIRE)	Time series is mostly gaps
JAFL (BanglaPIRE)	Insufficient data length
JAML (BanglaPIRE)	Insufficient data length
KHUL (BanglaPIRE)	Time series is mostly gaps
PUST (BanglaPIRE)	Time series is mostly gaps
RAJS (BanglaPIRE)	Time series is mostly gaps

Table S1: Blacklist of unused GNSS stations for hydrological loading analysis.

Table S2: Amplitude, phase, and velocity results for various models and the GNSS observations from MIBB and BanglaPIRE stations (included as separate text file).